FINAL REPORT ON THE

INTEREST JINR University Centre Wave 6 program

The crystal and magnetic structure of advanced oxide materials: neutron diffraction studies

Supervisor:

Nadezhda Belozerova

Student:

Marko Jelić, Vinča Institute of Nuclear Sciences, University of Belgrade, Serbia

Participation period:

14 February – 01 April, 2022

Abstract

In this work, we calculated structural and magnetic properties of doped spinel ferrite $Zn_{0.3}Cu_{0.7}Fe_{1.5}Ga_{0.5}O_4$. Starting from the time of flight (TOF) neutron diffraction data, Rietveld analysis was performed and parameters like lattice constants, atomic coordinates, interatomic distances and angles and magnetic moments were obtained. The diffraction patterns were recorded in the 297 K – 424 K range of temperature and 0.8 GPa – 3.4 GPa range of pressures. By increasing the temperature and the pressure, a gradual suppression of the magnetic moments of iron ions in both A and B crystallographic sites was observed. This effect corresponds to a magnetic phase transition from the ferrimagnetic state to paramagnetic. Besides changes in magnetic properties, ferrite showed interesting dependence of its structural parameters with temperature and pressure.

Contents

1.Introduction

Progress in modern condensed matter physics and the development of modern technologies in recent decades is inseparably connected with the studies of complex oxide materials, since in this class of compounds was discovered such important phenomena as high temperature superconductivity[1], giant magnetoresistance effect[2], the metal-insulator transition[3], charge [4] and orbital ordering[5], ferroelectricity[6], magnetoelectric effect[7], spin crossover[8], etc. The study of transition metal oxides (TMO), especially spinel ferrites which have many applications, is of great interest from both fundamental and applied research points of view[9]. Metal cations in such structures are distributed between two crystallographic positions: tetrahedral and octahedral (**Figure 1**). According to the distribution of cations, there are several types of ferrospinel structures: normal spinel structure, reverse spinel structure, mixed spinel structure[10]. Quite a large number of studies have been carried out on the spinel systems with varying different dopants and compostions[11–16]. Nevertheless, many aspects of the complex magnetic behavior relating to the structural changes arising from substitution of different magnetic and non-magnetic cations in spinels are yet to be resolved. It is well known that the magnetic interaction J_{AB} between the magnetic moments of iron in tetrahedral A and octahedral B sublattice are stronger than those between the moments of the ions in either tetrahedral sublattice J_{AA} or octahedral sublattice J_{BB}. A substitution by diamagnetic ions suppresses the magnetic coupling J_{AB} and changes drastically the balance between competing interactions J_{AA} and J_{BB}. Moreover, the magnetic properties of spinel ferrites can be affected by the cation–cation interactions between transition metal ions at B-sites. Neutron diffraction is the most direct and informative method of studying the magnetic ordering in crystal materials and can provide a clear picture of magnetic structures in disordered systems since it can manifest direct evidence of magnetic long range order (LRO) and short range order (SRO) and their cause by simple changes in nature and concentration of non-magnetic atoms in magnetic lattice while avoiding the effect of magnetic domains[17].

In the present work, Rietveld analysis based on structure refinement has been adopted for compound $Zn_{0.3}Cu_{0.7}Fe_{1.5}Ga_{0.5}O_4$ to determine several parameters: lattice constants, atomic

coordinates, interatomic distances and angles and magnetic moments. The structural and magnetic properties of doped ferrite have been studied using the method of neutron diffraction at high pressures up to 3.4 GPa and in temperature range 300–425 K. Software used for the refinement was FullProf.

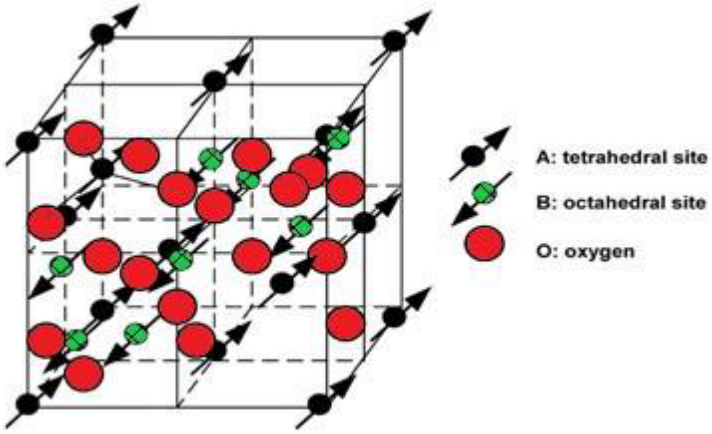

Figure 1. Representation of the general magnetic structure of spinel

2.Neutron diffraction

The neutron was discovered by James Chadwick in 1932, and after four years the diffraction of the neutron beam was demonstrated as a result of its scattering by the sample. The concept of Bragg diffraction applies equally to neutron diffraction and electron diffraction processes.

W.H.Bragg, W.L.Bragg and independently of them Y.V. Wulff pointed that a consequence of three dimensional periodicity of a crystal is that it can be divided into various sets of equidistant parallel planes containing identical atomic arrangements. They discovered that the geometry of the X-ray diffraction is similar to the reflection of light by a plane mirror. It is of course follows that the angle between incident ray and reflected ray is 2θ. Thus, the words diffraction and reflection are interchangeable in Wulff - Bragg's law.

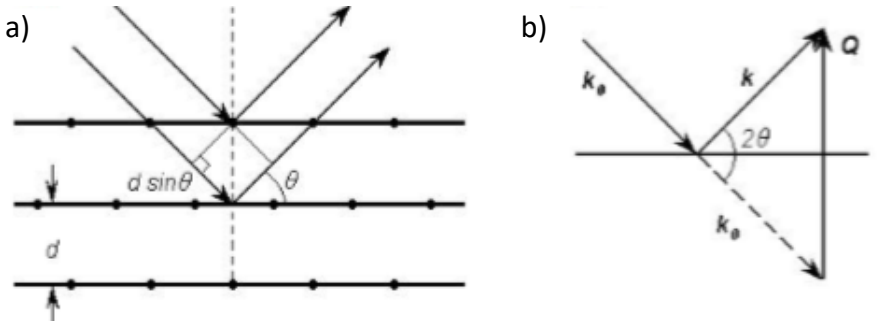

Figure 2. Bragg reflection from the set of planes with an inter planer spacing of 'd', θ is Bragg angle (a), triangle of neutron scattering (b)[9]

According to Wulff - Bragg's law if the set atomic planes have an inter planer spacing of 'd' and a monochromatic neutron beam of wavelength λ is allowed to incident on the plane with an

angle θ and is reflected back with the same angle then for constructive interference between the incident and reflected rays the path difference must be the integral multiple of wavelength i.e.

$$2d \cdot \sin\theta = n\lambda \tag{1.1}$$

where n =0, 1, 2, 3 ... represents the order of reflection, λ is de Broglie wavelength of neutron $\lambda = \frac{h}{mv} = \frac{h}{p} = \frac{h}{\sqrt{2mE}}$

The equation (1.1) is known as Wulff - Bragg's law. That equation can be written in another form, if the total neutron scattering is measured consisting of elastic scattering. It mean, wave vectors of incident and reflected neutrons are equal, and therefore $|\vec{k}| = |\overrightarrow{k_0}|$ (Fig. 1 (b)). Defining the scattering wave vector $\vec{Q} = \vec{k} - \overrightarrow{k_0}$ the diffraction condition can be written as

$$\vec{\mathrm{Q}} = \left|\vec{k} - \overrightarrow{k_0}\right| = 2\mathrm{k}\sin\theta = 4\pi \cdot \sin\theta/\lambda, \tag{1.2}$$

where λ is wavelength of incident neutrons. Seeing that the interplanar distance of reciprocal lattice $d = 1/|\vec{H}|$ then

$$\delta(\vec{\mathrm{Q}} - 2\pi{\cdot}n\,\vec{H}). \tag{1.3}$$

Equation (1.3) is another statement for the Wulff-Bragg's law.

Considering the interaction of a neutrons with a nucleus is described by the Fermi potential

$$V = \frac{2\pi h^2}{m} b \cdot \delta(\vec{r} - \vec{R}), \quad (1.4)$$

where $\vec{R}$ is the spatial value of the nucleus. It can be shown that the neutron diffraction cross section on the crystal has the following form

$$\left(\frac{d\sigma}{d\Omega}\right)_{\text{ког}} = \frac{(2\pi)^3}{V_0} \sum_H \delta(\vec{Q} - 2\pi \cdot n) \cdot |F(\vec{H})|^2, \quad (1.4)$$

where V_0 is volume of unit cell. Thus, the diffraction peaks of neutron scattering, which the intensity goes proportional to $\left|F(\vec{H})\right|^2$, will be observed, when the scattering wave vector is a vector of the reciprocal lattice.

$$F(H) = \sum_j b_j \exp\left(2\pi \cdot i\vec{H}\vec{r_j}\right), \quad (1.5)$$

where b_j is the coherent amplitudes of neutron scattering, $\vec{r_j}$ is coordinates of atoms in the cell.

2.1. Time of flight method

The time of flight (TOF) method is one of the main methods of neutron diffraction analysis. In our days, this is one of the most efficient method in structural neutronography.

The principal schema of a TOF diffraction experiment is shown in Figure 3.

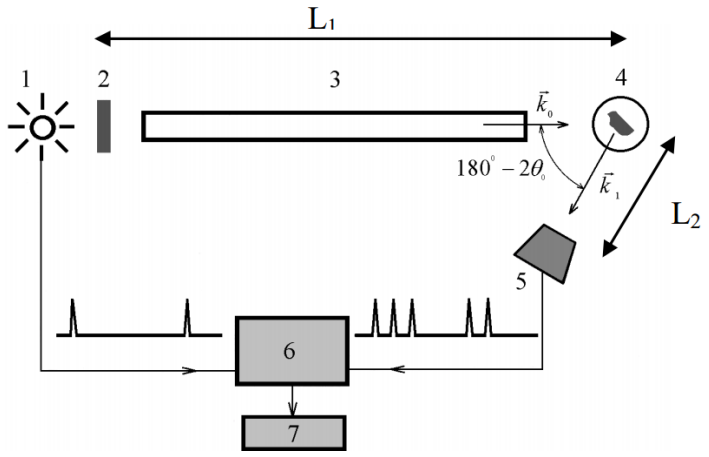

Figure 3. The lay-out of a TOF diffraction experiment: 1 – pulsed neutron source, 2 – moderator, 3 – flight path of the primary beam, 4 – sample, 5 – detector, 6 – time analyzer, 7 – RW memory[10]

The detector signal is stored in a multichannel time analyzer which is started synchronously with each pulse emission. Thus, the spectrum of recorded counts is built up in dependence on neutron flight time[11].

Neutrons possess the kinetic moment p

$$p = mv = \frac{h}{\lambda}, \quad (1.6)$$

where m is the neutron mass and v its velocity. In this way, the wavelength of neutron

$$\lambda = \frac{h}{mv}. \quad (1.7)$$

On the other hand, the velocity of the neutrons can be obtained from measurement of their flight times (t)

$$v = \frac{L_0 - L_1}{t}. \quad (1.8)$$

The wavelength of neutron can be written as

$$\lambda = \frac{ht}{m(L_0 + L_1)}. \quad (1.7)$$

Reflection occurs from system of parallel crystalline planes with Miller indices (hkl) at a fixed θ_0 and λ. The interplanar distance d_{hkl} should measure up of Wulff-Bragg's low:

$$2d_{hkl}sin\theta_0 = \lambda$$

Combining above equations yields a relation between the time of flight and interplanar d-spacing between lattice planes:

$$d_{hkl} = \frac{ht}{2m(L_0 + L_1)sin\theta_0}. \quad (1.8)$$

Scattered neutrons corresponding to the defined d_{hkl} can be easily separate due to the registration time. The time are fixing by the special equipment (time analyzer) which characterized by the number of time channels and they width. The reference-start point is correspond with the special start pulse coincided with neutron flare. Neutron diffraction patterns, obtained such way, represent time-resolved diffraction spectra. The range of wavelengths are widely used on the TOF diffractometeres, generally 0,9 – 8Å, in real life it can achieve 20 Å, which can partially compensate the reduction of neutron flux at long wavelengths.

The resolution of the TOF diffractometer is given as

$$R = \frac{\Delta d}{d} = \left(\left(\frac{\Delta t}{t}\right)^2 + (ctg\theta\Delta\theta)^2\right)^{1/2}, \quad (1.9)$$

where Δt is equivocation of time of flight and $\Delta\theta$ is geometric equivocation of dispersal process.

The advantages of TOF-diffraction are manifold increase of the factor of using neutrons from the source in comparison with the other neutron methods and the ability to conduct

measurements in a fixed geometry, while working with high pressure cells. The main disadvantage usually is the relatively less precision of the measurements.

3.1. FullProf

The program has been mainly developed for Rietveld analysis of neutron (nuclear and magnetic scattering) or X-ray powder diffraction data collected at constant or variable step in scattering angle 2θ. Two versions of the source code exist at present. The first corresponds to a source written in standard FORTRAN 77 (F77) language, and is organized as to be easily adapted to different computers. The second version of the source code has been developed from the previous one, and it has been totally re-written in a subset (ELF90) of the new standard Fortran 95 (F95).

Some of the most important features of FullProf are: X-ray diffraction data: laboratory and synchrotron sources; Neutron diffraction data: Constant Wavelength (CW) and Time of Flight (TOF); One or two wavelengths (eventually with different profile parameters); The scattering variable may be 2θ in degrees, TOF in microseconds and Energy in KeV; Background: fixed, refinable, adaptable, or with Fourier filtering; Choice of peak shape for each phase: Gaussian, Lorentzian, modified Lorentzians, pseudo-Voigt, Pearson-VII, Thompson-Cox-Hastings (TCH) pseudo-Voigt, numerical, split pseudo-Voigt, convolution of a double exponential with a TCH pseudo-Voigt for TOF; Multi-phase (up to 16 phases); Preferred orientation: two functions available; Absorption correction for a different geometries. Micro-absorption correction for Bragg-Brentano set-up; Choice between three weighting schemes: standard least squares, maximum likelihood and unit weights; Choice between automatic generation of hkl and/or symmetry operators and file given by user; Magnetic structure refinement (crystallographic and spherical representation of the magnetic moments). Two methods: describing the magnetic structure in the magnetic unit cell of making use of the propagation vectors using the crystallographic cell. This second method is necessary for incommensurate magnetic structures; Automatic generation of reflections for an incommensurate structure with up to 24 propagation vectors. Refinement of propagation vectors in reciprocal lattice units; hkl-dependence of FWHM

for strain and size effects; hkl-dependence of the position shifts of Bragg reflections for special kind of defects; Profile Matching. The full profile can be adjusted without prior knowledge of the structure (needs only good starting cell and profile parameters); Quantitative analysis without need of structure factor calculations; Chemical (distances and angles) and magnetic (magnetic moments) slack constraints. They can be generated automatically by the program; The instrumental resolution function (Voigt function) may be supplied in a file. A microstructural analysis is then performed; Form factor refinement of complex objects (plastic crystals); Structural or magnetic model could be supplied by an external subroutine for special purposes (rigid body TLS is the default, polymers, small angle scattering of amphifilic crystals, description of incommensurate structures in real direct space, etc); Single crystal data or integrated intensities can be used as observations (alone or in combination with a powder profile); Neutron (or X-rays) powder patterns can be mixed with integrated intensities of X-rays (or neutron) from single crystal or powder data; Full Multi-pattern capabilities. The user may mix several powder diffraction patterns (eventually heterogeneous: X-rays, TOF neutrons, etc.) with total control of the weighting scheme; Montecarlo/Simulated Annealing algorithms have been introduced to search the starting parameters of a structural problem using integrated intensity data.

Input files have different extensions like:

- FILE.pcr – input control file
- FILE.dat – input data files
- FILE.bac – background file
- FILE.hkl – reflection file
- FILE.irf – instrument resolution file
- FILE.shp – numerical profile file
- FLE.cor – intensity correction file
- FILE.int – reflection file

As a result of calculations connected to these files one can get results summarized in different output files:

- CODFIL.out - main output file that contains all control variables and refined parameters.
- CODFIL.prf – contains observed and calculated profile that can be fed into visualization programs. It can be automatically used by WinPLOTR.
- CODFIL.rpa – contains summary of refined parameters and it is useful when running FullProf in cyclic modes.
- CODFIL.sym – contains list of symmetry operators
- CODFIL.sum – contains parameter list after last cycle
- CODFIL.fou – contains different information about structural factors and can be used for (G)FOURIER and FOURTK programs
- CODFIL.ins – template of the input control file for the program SHELXS
- CODFIL.inp – template for (G)FOURIER input file
- CODFIL.hkl – list of reflections and can be input or output file
- CODFIL.sav – contains list of reflections between two selected angles and can be output file if an interval in the scattering variable is given
- CODFIL.dis – contains list of distances and angles for specific phase
- DCONSTR.hlp – list of strings containing eventual distance and angle constraints for specific phase
- CODFIL.mic – contains microstructural information
- CODFIL.sim – contains a simulated diffraction pattern. Can be renamed as a DAT file and used for refinement in simulation work.
- CODFIL.sub – contains calculated profile corresponding to the phase n
- CODFIL.atm – depending on a parameter *Jdi* it contains information about presence of magnetic phase, magnetic atom positions and can be used as input file for MOMENT program that calculates everything concerned with magnetic structures
- CODFIL.sch - files suitable as input files for programs SCHAKAL and STRUPLO

- CODFIL.int – files suitable as input files for integrated intensity refinements and contains a list of overlapped reflections obtained by adding integrated intensities from profile matching refinement when they belong to a cluster.

As it was mentioned in the short explanation of output files, there is connection between FullProf and many other programs. So information obtained from FullProf calculation can be used as input file for programs like (G)Fourier, WinPLOTR, DicVol, MOMENT, SCHAKAL, STRUPLO, VESTA etc. and vice versa. In the following text you can see some of the features that can be found in WinPLOTR and it's connection to FullProf[18].

3.2. WinPLOTR

WinPLOTR is a software used for visualization and analysis of powder diffraction patterns. It can be used to plot raw or normalized data files coming from neutron and X-ray diffractometers as well as Rietveld files created by Rietveld type refinement programs such as FullProf. WinPLOTR has been developed to be a preferential graphic interface for Rietveld type FullProf program and can also be used as GUI for programs that are frequently used in powder diffraction data analysis such as DicVOL, TREOR, ITO. There are many other features that can be found in WinPLOTR, such as: automatic peak search; automatic background points search; one can choose different X space and do different calculations like summation, difference, smoothing, derivation, background subtraction, profile fitting, FWHM calculations, microstructural analysis etc[19].

4. Experimental methods

A powder sample of $Zn_{0.3}Cu_{0.7}Fe_{1.5}Ga_{0.5}O_4$ ferrite was synthesized through solid-state reactions using Fe_2O_3, ZnO, CuO and Ga_2O_3 (with purity 99.99%) as starting materials[20]. The mixture of the oxide powders was annealed at 1100 ^{0}C within 72 h. The obtained material was milled and annealed again at the same temperature conditions to improve homogeneity. The final powders were pressed into pellets and sintered at 1200 ^{0}C for 8 h[20]. Neutron powder diffraction measurements at ambient and high pressures up to 3.4 GPa were performed at ambient temperatures with the DN-6 diffractometer at the IBR-2 high-flux pulsed reactor (Frank

Laboratory of Neutron Physics, Joint Institute for Nuclear Research, Dubna, Russia) using the sapphire anvil high-pressure cell[21] and TOF method. Several tiny ruby chips were placed at different points on the sample surface and the pressure was determined by a standard ruby fluorescence technique[22]. Diffraction patterns were collected at scattering angle $2\theta = 90^0$ with the resolution Dd/d = 0.012 at d = 2 Å. In addition, the sample $Zn_{0.3}Cu_{0.7}Fe_{1.5}Ga_{0.5}O_4$ was heated up to 425 K by means of special heater. The temperature was measured by the K-type thermocouple.

5. Results and discussion

5.1. Temperature dependences

Neutron diffraction patterns of $Zn_{0.3}Cu_{0.7}Fe_{1.5}Ga_{0.}5O_4$ measured at different temperatures are shown on **Figure 4**. The interatomic bond lengths and angles for the tetragonal and octahedral oxygen coordination as a function of temperature are presented in **Figure 5**. By increasing the temperature, Fe_A–O bond length, which characterizes the tetrahedral oxygen coordination around A-site, linearly decreases. In contrast, the Fe_B–O bond length of B-site oxygen coordination increases. Same trend as for Fe_A–O bond length was present for angular dependence (**Figure 5b**). Temperature dependence of the unit cell volume of $Zn_{0.3}Cu_{0.7}Fe_{1.5}Ga_{0.5}O_4$ spinel is shown in **Figure 6**. With temperature increase volume of the ferrite gradually grew.

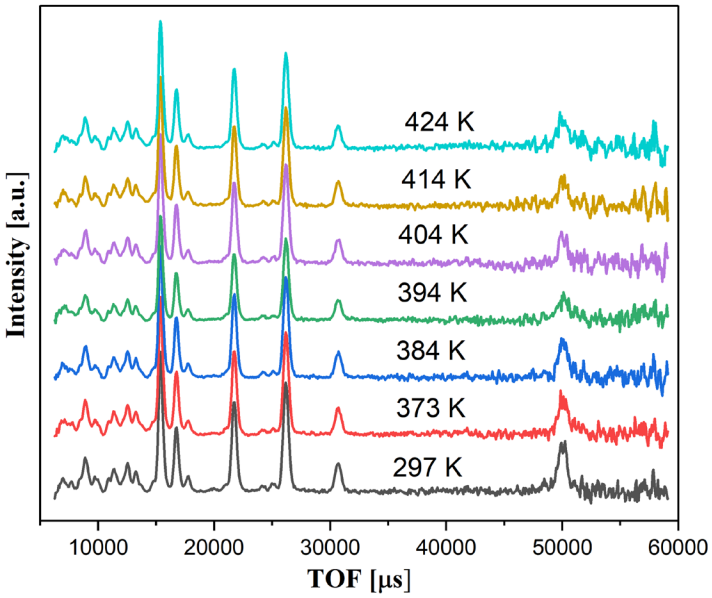

Figure 4. Neutron diffraction patterns of $Zn_{0.3}Cu_{0.7}Fe_{1.5}Ga_{0.5}O_4$ compound measured at selected temperatures up to 424 K.

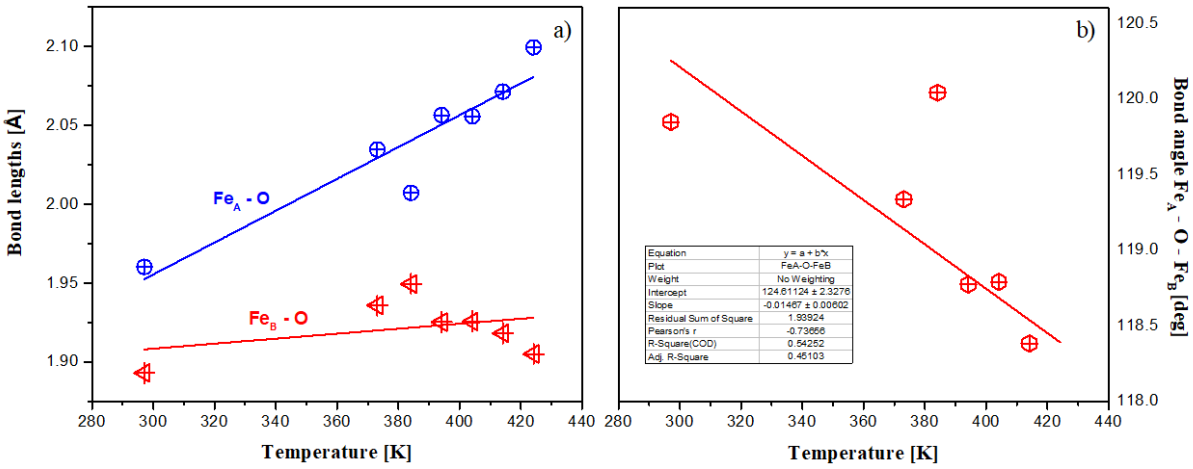

Figure 5. a) Fe_A–O and Fe_B–O bond lengths of $Zn_{0.3}Cu_{0.7}Fe_{1.5}Ga_{0.5}O_4$ as a function of temperature. The solid line represents a linear fit to the experimental data. (b) Fe_A–O–Fe_B bond angle of $Zn_{0.3}Cu_{0.7}Fe_{1.5}Ga_{0.5}O_4$ spinel as a function of temperature. The solid line represents a linear fit of the experimental data

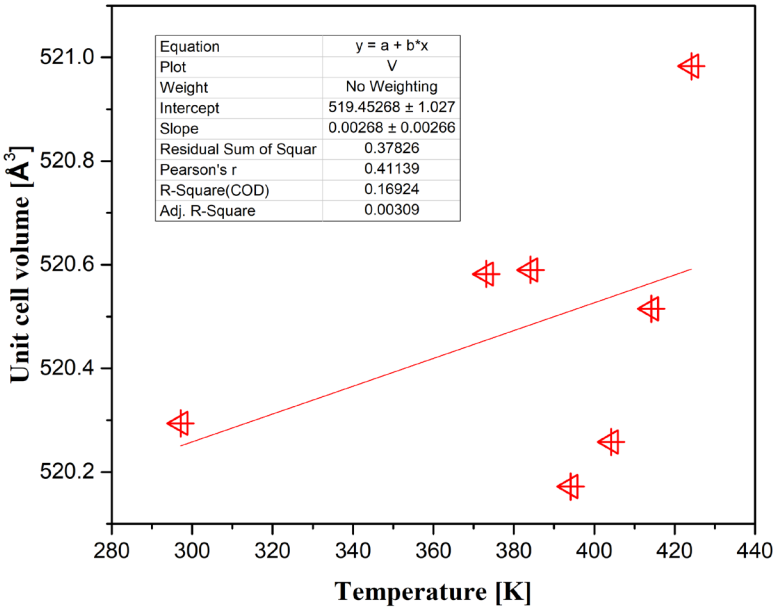

Figure 6. Temperature dependence of the unit cell volume of $Zn_{0.3}Cu_{0.7}Fe_{1.5}Ga_{0.5}O_4$ spinel. The solid line is linear fit of experimental data.

From the neutron diffraction data analysis at room temperature, the values of iron magnetic moments at different sites were determined, where $M_A = 3.24\ \mu_B$ for Fe ions located at the A sites and $M_B = 2.67\ \mu_B$ for those distributed in the B sites. The temperature dependencies of the ordered Fe magnetic moments in both crystallographic sites are shown in **Figure 6**. For higher temperatures, a gradual decrease of intensities of the diffraction peaks (111) at t≈25000 μs and

(222) at t≈50000 μs was observed, indicating a magnetic phase transition from ferrimagnetic state to paramagnetic one[11](**Figure 4**). From the neutron diffraction data analysis, temperature dependences of iron magnetic moments at different sites were determined.

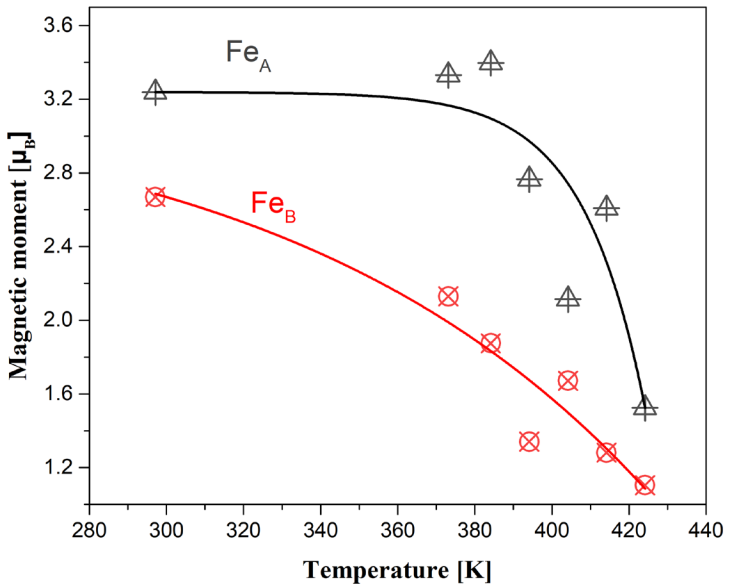

Figure 7. Temperature dependences of the magnetic moments of iron ions Fe_A and Fe_B located in A and B sites, respectively.

5.2. Pressure dependences

Neutron diffraction patterns of $Zn_{0.3}Cu_{0.7}Fe_{1.5}Ga_{0.5}O_4$ measured at different temperatures are shown on **Figure 8.**

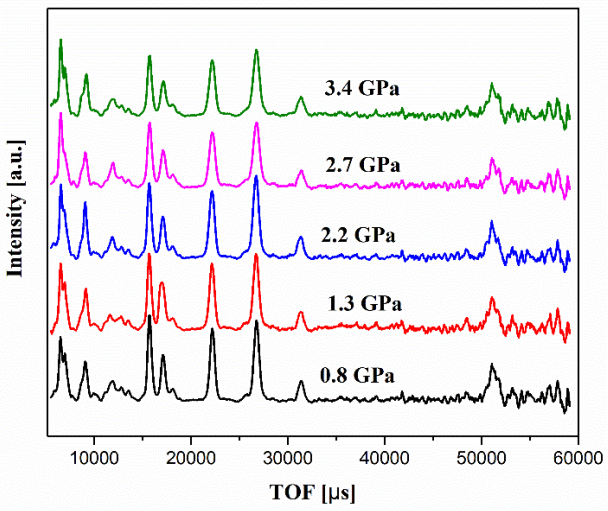

Figure 8. Neutron diffraction patterns of $Zn_{0.3}Cu_{0.7}Fe_{1.5}Ga_{0.5}O_4$ compound measured at selected pressures up to 3.4 GPa

Under compression, the bond length Fe_A–O increase and Fe_B-O bond length of $Zn_{0.3}Cu_{0.7}Fe_{1.5}Ga_{0.5}O_4$ compound decrease linearly (**Figure 9**). In the studied pressure range, the bond angle FeA-O-FeB controlling magnetic interactions between the A and B sublattices are slightly changed. The potential decrease of the FeA-O-FeB bond angle could cause the weakening of the Fe_A-O-Fe_B superexchange interactions by increasing the applied pressure. At a certain pressure, the Fe_A-O-Fe_B superexchange interaction may become comparable with those of the Fe_A-O-Fe_A and Fe_B-O-Fe_B interactions[11,23].

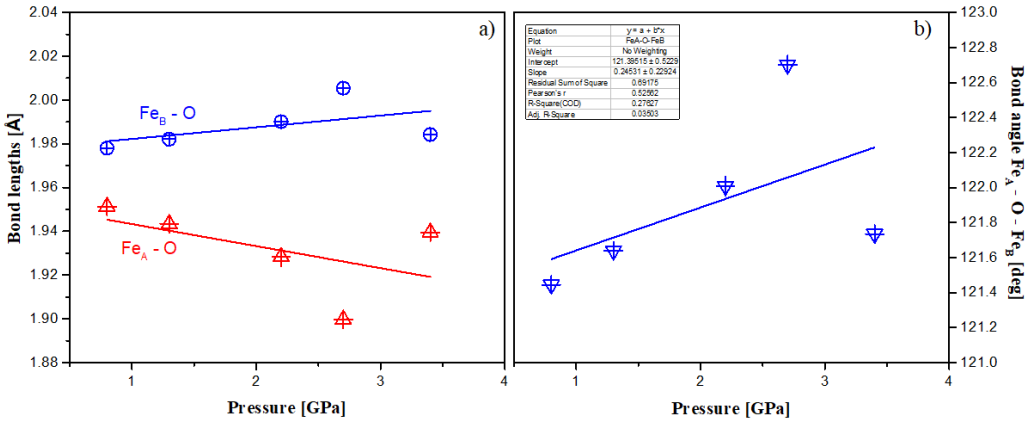

Figure 9. a) Fe_A–O and Fe_B–O bond lengths of $Zn_{0.3}Cu_{0.7}Fe_{1.5}Ga_{0.5}O_4$ as a function of pressure. The solid line represents a linear fit to the experimental data. (b) Fe_A–O–Fe_B bond angle of $Zn_{0.3}Cu_{0.7}Fe_{1.5}Ga_{0.5}O_4$ spinel as a function of pressure. The solid line represents a linear fit of the experimental data

From **Figure 10** could be concluded that lattice parameters and volume of the cell were not showing any trend as pressure grew.

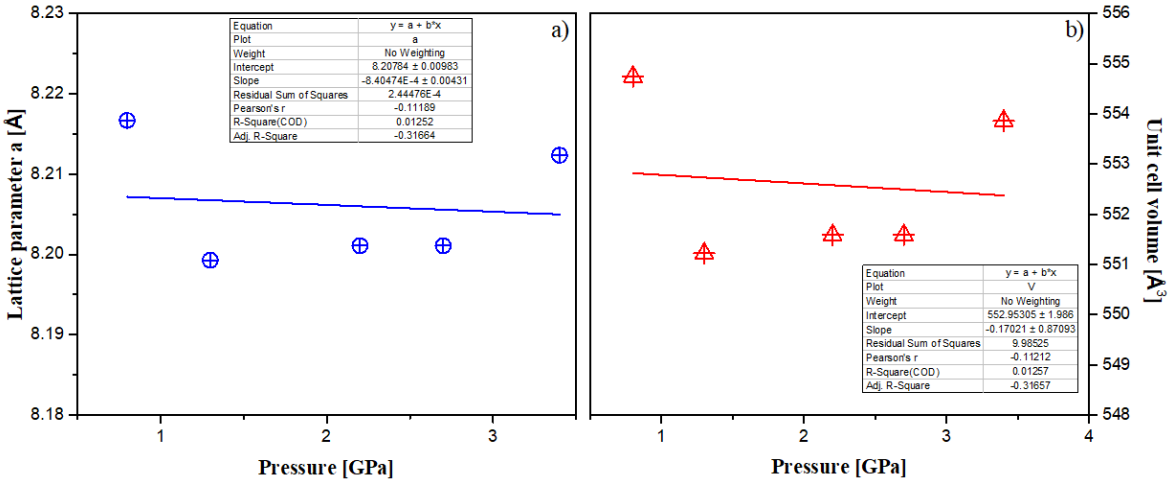

Figure 10. (a) The pressure dependence of the cubic lattice parameter fitted by linear functions. (b) The pressure dependence of unit cell volume of $Zn_{0.3}Cu_{0.7}Fe_{1.5}Ga_{0.5}O_4$ compound fitted by fitted by linear functions

The volume compressibility data were fitted by the third-order Birch–Murnaghan equation of state[24]:

$$P = \frac{3}{2}B_0(x7/3x5/3)[1 + ¾(B'4)(x2/31)] \quad (2.0)$$

where $x = V/V_0$ is the relative volume of unit cell and V_0 is the unit cell volume at P = 0; B_0 and B' are the bulk modulus $B_0 = -V\,(dP/dV)T$ and its pressure derivative $B0 = (dB0/dP)_T$. The best fit is achieved by B_0 = 76.30 GPa and B' = 4.

As illustrated in **Figure 12**, by increasing the pressure, the intensity of the magnetic peaks gradually decreases. At 0.8 GPa, M_A = 3.95 μ_B for Fe ions located at the A sites and M_B = 2.89 μ_B for those distributed in the B sites while at 3.4 GPa M_A = 2.65 μ_B and M_B = 2.10 μ_B. From the neutron diffraction data presented in **Figure 8**, slight decrease of the magnetic peak at t≈50000 μs was observed.

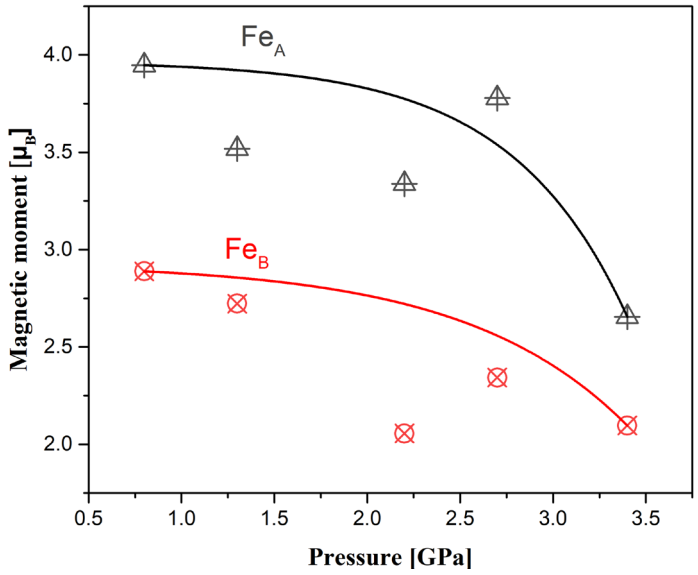

Figure 11. Temperature dependences of the magnetic moments of iron ions Fe_A and Fe_B located in A and B sites, respectively

6. Conclusion

In summary, we studied the crystal and magnetic structure of doped spinel ferrite $Zn_{0.3}Cu_{0.7}Fe_{1.5}Ga_{0.5}O_4$ at different temperatures and pressures. TOF diffraction patterns were collected with the DN-6 diffractometer at the IBR-2 high-flux pulsed reactor and Rietveld analysis was performed using FullProf software. After refinement, results indicated that examined compound exhibit high level of dependence from ambient conditions. By increasing the temperature and the pressure, a gradual suppression of the magnetic moments of iron ions in both A and B crystallographic sites was observed. This effect corresponds to a magnetic phase transition from the ferrimagnetic state to paramagnetic. Also, bond lengths, interatomic angles, volume of the cell were prone to change due to the different temperature and pressure conditions.

7. References

1. Tannhauser, D. S. Conductivity in iron oxides. *J. Phys. Chem. Solids* **23**, 25–34 (1962).

2. Rao, C. N. R. & Cheetham, A. K. Giant magnetoresistance in transition metal oxides. *Science (80-.).* **272**, 369–370 (1996).
3. Yang, Z., Ko, C. & Ramanathan, S. Oxide electronics utilizing ultrafast metal-insulator transitions. *Annu. Rev. Mater. Res.* **41**, 337–367 (2011).
4. Coey, M. Condensed-matter physics: charge-ordering in oxides. *Nature* **430**, 155–157 (2004).
5. Tokura, Y. & Nagaosa, N. Orbital physics in transition-metal oxides. *Science (80-.).* **288**, 462–468 (2000).
6. Li, W. *et al.* Ferroelasticity in a metal-organic framework perovskite; Towards a new class of multiferroics. *Acta Mater.* **61**, 4928–4938 (2013).
7. Birol, T. *et al.* The magnetoelectric effect in transition metal oxides: Insights and the rational design of new materials from first principles. *Curr. Opin. Solid State Mater. Sci.* **16**, 227–242 (2012).
8. Orlov, Y. S., Nikolaev, S. V. & Ovchinnikov, S. G. Magnetic Properties and Spin Crossover in Transition Metal Oxides with d 5 Ions at High Pressures. *J. Exp. Theor. Phys.* **129**, 1062–1069 (2019).
9. Valenzuela, R. Novel applications of ferrites. *Phys. Res. Int.* **2012**, (2012).
10. Vojt_ech, C. Hyper ne Interactions in Ferrites with Spinel Structure Ph.D. Thesis. (Prague University, 2010).
11. Kaiser, M. & Ata-Allah, S. S. Mössbauer effect and dielectric behavior of NixCu0.8-xZn0.2Fe2O4 compound. *Mater. Res. Bull.* **44**, 1249–1255 (2009).
12. Moussaoui, H. El, Masrour, R., Mounkachi, O., Hamedoun, M. & Benyoussef, A. Cation distribution and magnetic interactions in ZN-substituted Fe(Cu)Fe2O4 ferrites. *J. Supercond. Nov. Magn.* **25**, 2473–2480 (2012).
13. Birajdar, A. A. *et al.* Rietveld Structure Refinement and Cation Distribution of Substituted Nanocrystalline Ni-Zn Ferrites. *ISRN Ceram.* **2012**, 1–5 (2012).
14. Al-Haj, M. Microstructure characterization of ZnFe2-xMxO 4 (M = Bi, Y and x = 0.1, 0.2) ferrites by the rietveld refinement. *Turkish J. Phys.* **29**, 85–90 (2005).
15. Leung, L. K., Evans, B. J. & Morrish, A. H. Low-temperature mössbauer study of a nickel-

zinc ferrite: ZnxNi1-xFe2O4. *Phys. Rev. B* **8**, 29–43 (1973).

16. Fayek, M. K., Ata-Allah, S. S., Zayed, H. A., Kaiser, M. & Ismail, S. M. Effect of Zn substitution on relaxation characteristics and dielectric properties of Cu1-xZnxGa0.5Fe1.5O4 spinel. *J. Alloys Compd.* **469**, 9–14 (2009).
17. Yunus, S. M. *et al.* Neutron diffraction studies of the diluted spinel ferrite ZnxMg0.75-xCu0.25Fe2O4. *J. Magn. Magn. Mater.* **232**, 121–132 (2001).
18. Juan Rodriguez-Carvajal. An introduction to program FullProf. *Manual* (2001).
19. Roisne, T. & Rodriguez-Carvajal, J. WinPLOTR, a graphic tool for powder diffraction – Manual. (2001).
20. Ata-Allah, S. S. Influence of Ga substitution on the magnetic and electric behavior of Cu0.5Zn0.5Fe2O4 compound. *J. Magn. Magn. Mater.* **284**, 227–238 (2004).
21. N.M. Belozerova, Kichanov, S. E. & Jirák, Z. High pressure effects on the crystal and magnetic structure of nanostructured manganites La0.63Sr0.37MnO3 and La0.72Sr0.28MnO3. *J. Alloys Compd.* **646**, (2015).
22. Kozlenko, D. P. *et al.* Structural and magnetic phase transitions in Pr 0.15Sr 0.85MnO 3 at high pressure. *Eur. Phys. J. B* **77**, 407–411 (2010).
23. Ata-Allah, S. S. & Hashhash, A. Jahn-Teller effect and superparamagnetism in zn substituted copper-gallate ferrite. *J. Magn. Magn. Mater.* **307**, 191–197 (2006).
24. Birch, F. Equation of state and thermodynamic parameters of NaCl to 300 kbar in the high-temperature domain. *J. Geophys. Res.* **91**, 4949 (1986).